




Bessel beam propagation using radial beam propagation method at different propagation scales

ADEL S. A. ELSHARKAWI,^{1,2,4} I-CHEN TSAI,² XIANG-TING LIN,²
CHIA-YUAN CHANG,²  AND YU-LUNG LO^{2,3,*}

¹Department of Radiation Engineering, National Center for Radiation Research and Technology (NCRRT), Egyptian Atomic Energy Authority, Cairo 11787, Egypt

²Department of Mechanical Engineering, National Cheng Kung University, Tainan 701, Taiwan

³Academy of Innovative Semiconductor and Sustainable Manufacturing, National Cheng Kung University, Tainan 701, Taiwan

⁴11105043@gs.ncku.edu.tw

*loyl@ncku.edu.tw

Abstract: This paper is devoted to studying the Bessel beam propagation in cylindrical coordinates using the Hankel transform beam propagation method (HT-BPM) and their behavior in different scenarios in the microscale and meter scale of propagation distances. The study compares the results obtained from the HT-BPM with another fast Fourier transform beam propagation method (FFT-BPM) to validate the accuracy and effectiveness of the HT-BPM in modeling Bessel beam propagation. The axial intensity of Bessel beam propagation is analyzed using the HT-BPM. The simulation results obtained from the HT-BPM are compared with those from the FFT-BPM to evaluate the agreement and consistency between the two methods in predicting the axial intensity of Bessel beam propagation. The results show that the HT-BPM is numerically faster than the FFT-BPM by ten times for different sampling points, furthermore, the FFT-BPM accuracy for evaluating the Bessel beam spot radius is 89.9% of the analytical value, while the HT-BPM is 99% relative to analytical value. The prediction of the axial intensity of the Bessel beam has been tested at different types of phase functions and different propagation distances: micrometer, centimeter, and meter scales. The results of the HT-BPM are matched with the analytical and experimental values. Finally, the HT-BPM is tested when the input light source takes different profiles.

© 2024 Optica Publishing Group under the terms of the [Optica Open Access Publishing Agreement](#)

1. Introduction

Bessel beams exhibit unique properties such as resistance to diffraction and the ability to self-heal their intensity distribution after encountering obstacles [1]. These characteristics make them distinct from other types of beams and have been the focus of extensive research [2]. Bessel beams are generated through the superposition of plane waves that have constant inclined wave vectors lying on a cone of angle [3]. The self-healing and non-diffractive intensity distribution have led to their potential application in various fields, in material processing, they have been used for cutting or drilling [4,5]. The generation of the Bessel beam has been approached in various ways, including through direct methods and nonlinear wave-mixing processes. Other methods include the use of spatial light modulators (SLMs) or axicons to shape and control the beams more precisely [6]. Efficient methods for generating Bessel beams continue to be crucial for advancing research and applications in these various fields.

Durnin's groundbreaking [1,7] work in 1987 paved the way for understanding the Helmholtz equation in free space and its solutions in terms of Bessel functions. His studies showed that Bessel beams are exact non-diffracting solutions to the Helmholtz equation, which remain focused

over a certain distance without spreading out. The experimental generation of a zero-order Bessel beam using an annular slit aperture was indeed inefficient, as a significant portion of the beam's intensity was blocked [8,9]. This inefficiency has driven research towards more effective methods for creating Bessel beams. The theoretical properties of Bessel beams, recognized for their concentric radial rings and hypothetical unlimited energy, have been extensively studied, revealing complex modes with central dark areas or vortices [10]. In addition, SLM has played a crucial role in the development of Bessel beam generation. They allow for the tunable axicon hologram, providing a versatile tool for adjusting Bessel beam measurement ranges [8,11–13]. Combined spatial phase plates and axicon phase-only holograms, along with spiral phase holograms, have been used to generate higher-order Bessel beams, illustrating the versatility of SLM in beam shaping [8]. Studies have shown that the intensity distribution of Bessel beams generated through both a real axicon and an axicon hologram encoded in an SLM is similar [11], with beams produced by SLM maintaining a flawless shape throughout the range of propagation. These findings advocate for the use of simulated axicon holograms to generate scalar as well as vector Bessel beams, leveraging the benefits of SLM technology over physical axicons [14]. In addition, Bessel vortex beams with a helical phase structure can be achieved through a power-exponent-phase vortex of the Bessel beam. This approach allows for the construction of beams with unique vortex phases, which can be utilized in various applications [15–19].

In the realm of optics and laser technology, the beam propagation method (BPM) is a widely employed computational technique for simulating the propagation of light through diverse optical systems [20–22]. It enables researchers and engineers to analyze the characteristics of laser beams, such as their intensity distribution, and wavefront shape. The BPM relies on numerical solutions to Maxwell's equations using computational methods [23]. This method involves dividing the optical system into smaller segments and iteratively calculating the electric field distribution in each segment based on its interaction with neighboring segments. This iterative process continues until a stable solution is obtained, providing valuable insights into the propagation characteristics of the beam. The BPM is especially valuable in investigating the impact of diffraction, aberrations, and other optical phenomena on the propagation of laser beams. Moreover, it can be employed to optimize the design of optical systems by analyzing how changes in parameters such as beam size, focal length, and aperture influence the propagation characteristics of the beam.

In this work, the BPM has been studied in cartesian and polar coordinates for Bessel beam generation. The propagation of Bessel beams is accurately simulated using the HT-BPM in cylindrical coordinates and the FFT-BPM in cartesian coordinates. A comparison between HT-BPM and FFT-BPM in Bessel beam propagation reveals certain advantages of using the HT-BPM method.

2. Beam propagation method (BPM)

2.1. BPM algorithm for cartesian and radial coordinates

The propagation of Bessel beams is a topic of significant interest in various fields, including optics, telecommunications, and laser material processing [24]. In the BPM, an inhomogeneous medium is simulated as a series of lenses (lens-like medium) within a homogeneous medium [25,26]. The input Gaussian beam is modified by a phase-only function to generate the initial Bessel beam, altering only the imaginary part of the Gaussian beam. This generated Bessel beam is transformed into the spectral domain, multiplied by the propagator function, and then propagated over a small distance through the homogeneous medium. The FFT-BPM, also known as the spectral method, is a computational technique used to study the Bessel wave propagation. This method is particularly advantageous due to its efficiency in modeling the propagation of optical waves through complex and varied media [22]. Utilizing the Fast Fourier Transform (FFT) algorithm, this method can handle large-scale problems with relative ease, allowing for accurate simulation of wave behavior in challenging environments. Additionally, the FFT-BPM approach

is well-suited for simulating the generation of Bessel beams using a spatial light modulator (SLM), offering a powerful tool for studying and applying non-diffracting beams in various optical systems. However, it is important to note the drawbacks of the FFT-BPM approach. One limitation is the necessity for discretization, which can introduce numerical errors and impose restrictions on the resolution and scale of simulations. Furthermore, the method may require careful consideration and fine-tuning of parameters to accurately capture the subtleties of wave propagation in certain scenarios [27]. For a more accurate simulation of Bessel beam propagation, many scientists use the Wolf-Richardson (WR) equation [28] to evaluate Bessel beam propagation accurately. The propagation of Bessel beams is more accurately simulated using the HT-BPM in cylindrical coordinates rather than the FFT-BPM in Cartesian coordinates, as its structure is very similar to the WR equation in [27].

In addition, the HT-BPM method directly utilizes cylindrical coordinates, which are naturally suited for describing Bessel beams. This allows for a more accurate representation of the beam's radial intensity distribution [27]. By incorporating these effects, the HT-BPM method provides a more comprehensive and realistic simulation of Bessel beam propagation. Furthermore, the HT-BPM method allows for efficient propagation of Bessel beams with complex wavefronts or curved trajectories and shaping the Bessel beam axial intensity. This is achieved by utilizing the cylindrical symmetry of Bessel beams and accurately representing their propagation dynamics. However, the disadvantage of HT-BPM is that it is only limited to cylindrical symmetry beams such as Bessel beam [27,29].

For more investigations, the symmetric input Gaussian field is multiplied by the phase-only function (phase retardation function) as follows:

$$E(r) = e^{-\left(\frac{r}{w_0}\right)^2} e^{-j\varphi(r)} \quad (1)$$

where r is the radial position, $r = \sqrt{(x^2 + y^2)}$, and w_0 is the input Gaussian beam waist. The phase function $\varphi(r)$ could be written in different ways based on the Bessel beam generation technique, for example, in the case of axicon [30–32] as:

$$\varphi(r) = k_0 r (n - 1) \sin\theta \quad (2)$$

where k_0 is the wavevector in free space $k_0 = 2\pi/\lambda$, n is the axicon material refractive index, and θ is the cone angle of the wavevectors lying on the direction of propagation. The axicon (a cone lens) could be converted as diffractive grooves (i.e. diffractive optical element by its pixels) [11] with height h and depth d and could be simulated by using the SLM. Thus, the phase function can be written as [11]:

$$\varphi(r) = k_0(n - 1)r \frac{h}{d} \quad (3)$$

where $\theta = \arctan(h/d)$ is the base angle depends on groove height h and the groove period d , and n is the refractive index of the groove. The groove height h can be calculated as [11]:

$$h = \frac{\lambda}{n - 1} \quad (4)$$

For comparison between FFT-BPM and HT-BPM, Fig. 1(a) shows the flowchart of FFT-BPM, firstly, calculate the propagator functions based on the opto-geometric parameters. The result from Eq. (1) is transformed to the spectral domain using the Fourier transform and the results are multiplied by the propagator function ($P(k_r)$). These results are then transformed back to the spatial domain using the inverse Fourier transform and multiplied by the phase correction function ($Q(r)$) which is unity in the current case (free space propagation after the SLM or axicon), yielding the final Bessel beam distribution. These processes are repeated until the end of propagation length. However, in cylindrical coordinates, the propagator functions are calculated

using a different approach, considering the radial symmetry of the beam structure, furthermore, the transverse coordinates are only half of the used in the FFT-BPM case due to symmetry of the structure. Figure 1(b) shows the flowchart of HT-BPM. As shown, instead of using the Fourier transform and its inverse, the HT-BPM uses the Hankel transform and its inverse [33,34] and repeat the same process. This allows for a more efficient calculation of the propagator functions and enables the simulation of a Bessel beam with radial symmetry. It is noted that the Hankel transform kernels based on zeros of the Bessel function [33] should be calculated and saved at the beginning of the simulations in case the used numerical software languages did not offer the built-in Hankel transform functions. The absorbing guard boundary should be applied in both algorithms to remove any back reflections.

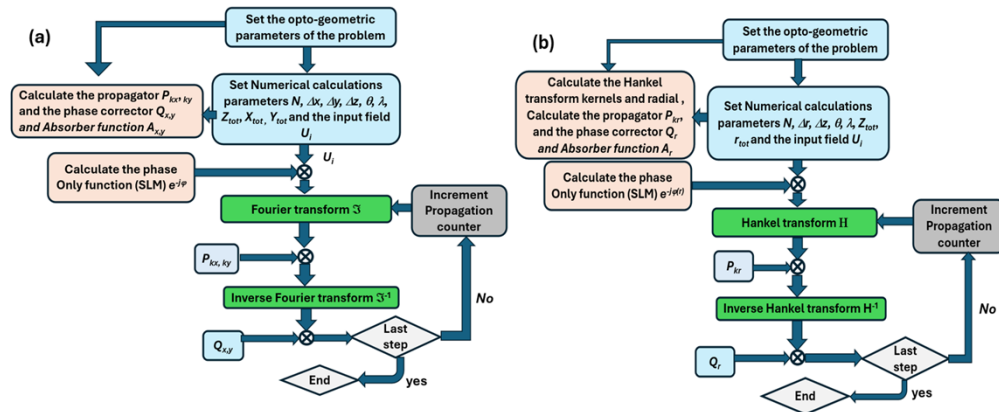


Fig. 1. BPM flowchart for both (a) FFT-BPM and (b) HT-BPM.

It is noted that the only difference between FFT-BPM and HT-BPM is the calculation of kernel functions [33]. Also, in the HT-BPM, the field is azimuthal and radial symmetric, consequently, half of the transverse window is sufficient to calculate the field distribution. This means that the HT-BPM can save computational resources compared to the FFT-BPM by only calculating half of the transverse window [33,35]. Furthermore, the time will be reduced significantly as the calculation of propagator functions in the HT-BPM is more efficient due to the use of Hankel transform and its inverse instead of the traditional Fourier transform and inverse transform.

Figure 2 shows the 3D plot for the Bessel beam propagation using the HT-BPM. This technique allows for the analysis and simulation of the propagation behavior of Bessel beams more efficiently and accurately. It is found that by using the HT-BPM, the complex propagation characteristics of Bessel beams can be accurately and efficiently studied and simulated. Furthermore, the HT-BPM method provides a comprehensive understanding of the beam's propagation behavior, including its intensity profile, phase distribution, and focal properties. As shown in Fig. 2's inset, the transverse profile of a Bessel beam generated using the HT-BPM exhibits a characteristic intensity maximum at the center, with concentric rings of decreasing intensity towards the outer edges. The axial intensity distribution of the Bessel beam remains invariant along the propagation direction. However, in the far region, the Bessel beam converted to be ring shape because of diffraction. This demonstrates the capability of the HT-BPM to accurately model and analyze the propagation of complex optical beams, such as Bessel beams, through different optical systems and investigate their behavior under various conditions [36].

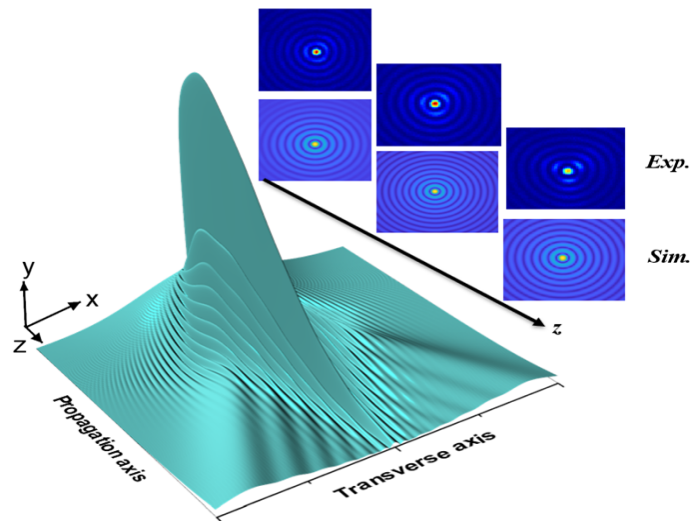


Fig. 2. 3D plot for the Propagated Bessel beam using the HT-BPM, the images of the propagated Bessel beam from numerical and experimental at different positions.

2.2. Comparison of execution time between FFT-BPM and HT-BPM

In the field of numerical simulations for optical fields, the choice between FFT-BPM and HT-BPM depends on various factors such as the specific requirements of the simulation, the computational resources available, and the complexity of the optical system being modeled. Figure 3 shows the execution time for simulations using FFT-BPM and HT-BPM at different numbers of sampling points. The execution time for the FFT-BPM is generally higher compared to the HT-BPM due to the more complex calculations involved in the Fourier transformation. Additionally, the computational complexity of the FFT-BPM increases with larger grid sizes and higher iteration numbers. However, it is important to note that the computational execution time can vary depending on the specific implementation of each method and the hardware used for simulations. Overall, the choice between FFT-BPM and HT-BPM should be based on careful consideration of the specific requirements of the simulation and the available computational resources. To evaluate the computational execution time, a comparison was made between FFT-BPM and HT-BPM simulations in the propagation of Bessel beams. We calculated the BPM serially using MATLAB code on a CPU with a 12th Gen Intel, Core i9-12950HX running at 2.30 GHz and 32.0 GB of RAM. Additionally, the MATLAB code has been implemented with the following initial parameters: an incident beam wavelength of 650 nm at a beam waist of 6 mm, a transversal window length of 0.02 m with an interval of $\Delta x = 39 \mu\text{m}$ in FFT-BPM and $\Delta r = 19 \mu\text{m}$ in HT-BPM, and a propagation length of 1.5 m with an interval of $\Delta z = 0.01$ m. The chosen propagation length is extended to test both the accuracy of the results and the speed. The simulation results showed that the HT-BPM had a shorter computational execution time compared to the FFT-BPM. Computational execution time is a crucial factor in determining the efficiency and feasibility of numerical simulations.

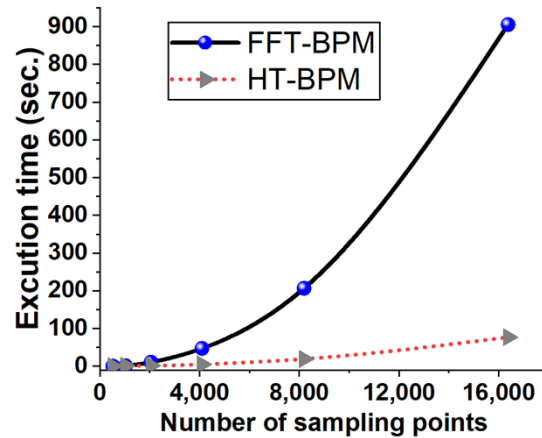


Fig. 3. Execution time comparison between FFT-BPM and HT-BPM at different number of sampling points.

3. Bessel beam at different propagation scales

3.1. Bessel beam generations in comparison between FFT-BPM and HT-BPM

The Bessel beam could be generated by different techniques such as: an annular aperture [7,37], Axicon lens [31,32,38], the diffractive optical element [39], metamaterials [40], and SLMs [11,41,42], which provides more flexibility and higher energy throughput. A computational comparison was conducted between the FFT-BPM and HT-BPM methods for generating Bessel beams. The computational execution time of the two methods was compared, and it was found that the HT-BPM method had a shorter execution time compared to the FFT-BPM method as presented in Fig. 3. This finding suggests that the HT-BPM method may be more efficient for generating Bessel beams in practical applications where computational speed is crucial. To support this conclusion, the experimental scans obtained from both methods were compared to predictions from an analytical model and experimental results. The Bessel beam, after being generated using SLM takes the form shown in Fig. 2's inset. In [11], the Bessel beam generated based SLM as diffraction grooves with d and h . The main loop radius [11] can be calculated as:

$$\rho_o = \frac{2.4048d}{k_o(n-1)h} \quad (5)$$

Figure 4 illustrates the Bessel main loop spot radius comparison between the FFT-BPM and HT-BPM at $d = 162.5 \mu\text{m}$, the refractive index $n = 1.51637$, the light beam wavelength $\lambda = 0.65 \mu\text{m}$, and $h = 1.2 \mu\text{m}$. As shown, the FFT-BPM accuracy is 89.9% of the analytical value, while the HT-BPM is 99% relative to the analytical value. This enhancement is crucial in applications like micromachining or laser ablation with femtosecond lasers utilizing Bessel beams, where surface roughness is a significant factor. In these applications, the diameter of the drilling holes ranges from 1 to 5 μm . Therefore, precise modeling is essential, and HT-BPM provides these advantages.

Additionally, Fig. 5 shows the Bessel beam spot radius at different values of groove period d . As shown, the HT-BPM is very close to the analytical values. Furthermore, in the figure inset the HT-BPM is smaller in relative error than the FFT-BPM to predict the Bessel beam spot radius. These results show that the HT-BPM is more accurate in Bessel beam propagation than the FFT-BPM.

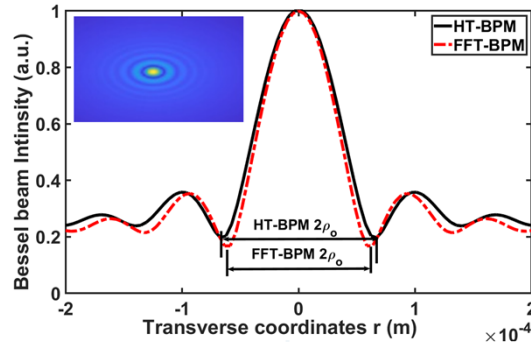


Fig. 4. Bessel beam field comparison between FFT-BPM and HT-BPM.

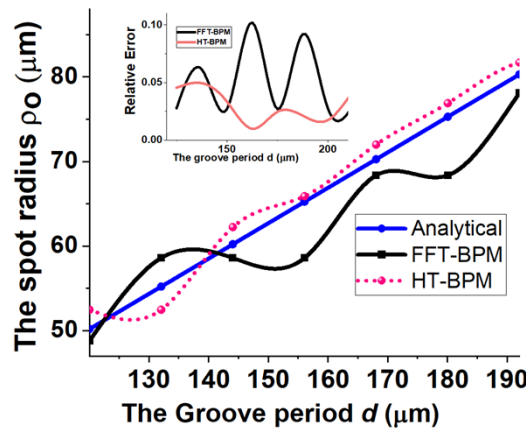


Fig. 5. Accuracy curve of predicting the Bessel beam spot radius comparison between HT-BPM and FFT-BPM. The inset is the relative error between FFT-BPM, HT-BPM, and analytical calculated from Eq. (5).

3.2. Axial intensity of Bessel beam in comparison between FFT-BPM and HT-BPM at meter scale using the model

Understanding the axial intensity of Bessel beams is important in various applications, such as optical tweezers [43–45], microscopy [46,47], and laser drilling [5,48–52]. Researchers and engineers continue to explore the properties and potential uses of Bessel beams in different fields, making them an interesting subject of study in the field of optics and photonics. To test the HT-BPM to simulate the Bessel beam propagation in meter scale, the analytical form of the Bessel beam intensity along the propagation direction z could be written as [11]:

$$I_{(z)} = 2A^2 \pi k_0 z \left(\frac{h}{d}\right)^2 (n-1)^2 \exp \left[-2 \left(\frac{(n-1)zh}{w_0 d} \right)^2 \right] I_0 \quad (6)$$

where I_0 is the intensity of the initial Bessel beam by squaring the results from Eq. (1) after the SLM or Axicon is normalized by $A = 1$.

Figure 6 shows the normalized axial intensity of the propagated Bessel beam, as shown in the figure both the BPM methods are compatible with the analytical and experimental values along the propagation direction as expected. However, the HT-BPM is more accurate than the

FFT-BPM, as shown in Fig. 6's inset, the relative error of the HT-BPM is very small compared to the FFT-BPM.

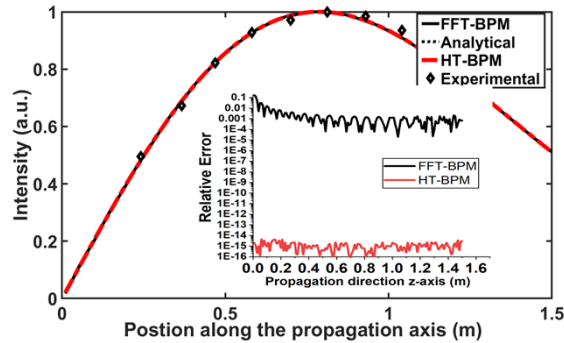


Fig. 6. Axial intensity of the Bessel beam along the propagation axis, the comparison between FFT-BPM and HT-BPM, analytical, and experimental results in [11].

3.3. Axial Intensity of Bessel beam in comparison between FFT-BPM and HT-BPM at micrometer scale

For more comparison, in real experiments to generate the Bessel beam after using SLM, the axial intensity distribution of the Bessel beam can be measured and analyzed. By using appropriate measurement arrangements and techniques, the axial intensity distribution of the Bessel beam can be quantified and studied in real experimental setups. In micro-drilling applications, in silicon packaging, the spot size of the Bessel beam should be in the range of 1 ~ 5 μm [51,53]. So, optical magnifications (telescope) should be used for the generated Bessel beam. After the telescope the propagation distances in a micrometer scale. The axial intensity could be calculated from the relation [30]:

$$I(z) = 8\pi I_0 n z \frac{\sin^2 \theta}{\lambda w_0^2} e^{-2\left(\frac{z \sin \theta}{w_0}\right)^2} \quad (7)$$

Figure 7 shows the axial intensity of the Bessel beam in the range of 50 μm . The BPM is in good agreement with analytical and experimental values. However, the HT-BPM will be suited to model the Bessel beam propagation as its relative error is smaller than the FFT-BPM as illustrated in Fig. 7 inset. Given the nature of HT-BPM being a radial coordinate, the results aligned with expectations that the relative error for HT-BPM would be significantly lower compared to FFT-BPM, which operates in Cartesian coordinates. Thus, numerical errors may arise from discretization and conversion between radial and Cartesian systems.

3.4. Experimental validation of using the HT-BPM in Bessel beam propagation at the centimeter scale

In this section, the validation of Bessel beam axial intensity using the beam propagation method is discussed. This validation involved comparing the results obtained from HT-BPM, FFT-BPM, and the analytical model. Furthermore, the experimental setup used for this validation included a laser source and optical components for beam shaping, ensuring precise control over the Bessel beam's characteristics and parameters. Figure 8(a) shows the block diagram of the experimental setup. The He-Ne laser has a wavelength of 632.8 nm, and the first polarizer (P1) is used to control the laser power. A spatial filter is adopted to produce a clean Gaussian beam and expand the beam size to nearly 8 mm. The second polarizer (P2) has a horizontal transmission axis to ensure the laser maintains the p polarization. The laser is normally incident to an SLM

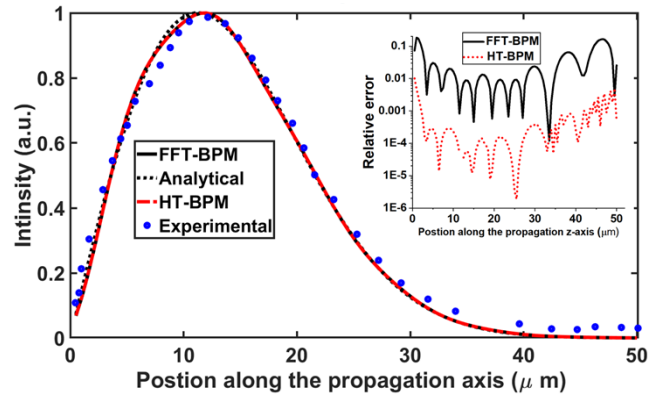


Fig. 7. Axial intensity of the Bessel beam along the propagation axis, and the comparison between FFT-BPM and HT-BPM, analytical, and experimental results from [30], as shown in the black line in the back of the red dashed line. The inset shows the relative error between FFT-BPM and HT-BPM with analytical calculated from Eq. (7).

(PLUTO-2.1-NIR-134, HOLOEYE Photonics, Germany) which is employed to generate a phase mask. The shaped laser beam is reflected by a beam splitter (BS) and finally recorded by a beam profiler (SP920s, Ophir Optonics) at different axial positions. Figure 8(b) shows the photographs of the system setup.

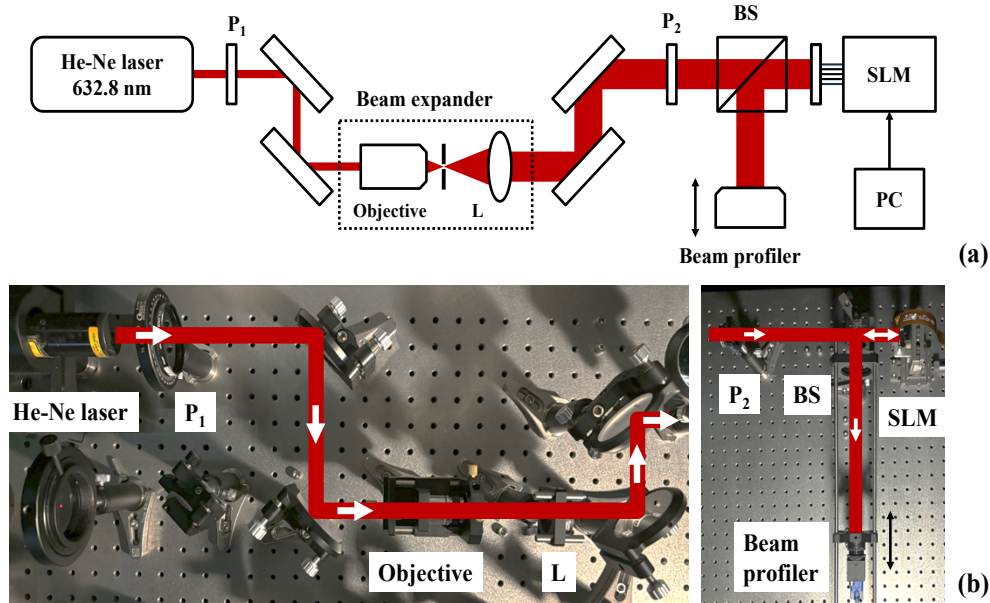


Fig. 8. The experimental setup for Bessel beam: (a) block diagram; (b) photograph.

Figure 9 shows the axial beam intensity profile along the propagation axis, and a comparison between the FFT-BPM, HT-BPM, analytical values from Eq. (6), and the measured values using the setup in Fig. 8(b) is illustrated. The observed shift in measurements occurs because the measurements commenced after the beam splitter depicted in Fig. 8(b). The validation results demonstrate strong concordance between the two methods, thereby verifying the accuracy

and dependability of employing the HT-BPM for Bessel beam modeling. Axial intensity measurements of the Bessel beam, conducted using a beam profiler, revealed that both methods produce highly consistent results. However, as illustrated in Fig. 9's inset, the HT-BPM is superior in accuracy and exhibits a lower relative error compared to the FFT-BPM. It is important to note that discrepancies between measured and simulated data may arise due to practical experimental issues. For instance, the actual beam shape could deviate from an ideal Gaussian beam, and despite precise alignment of the optical setup, the beam might still be incident at a slight angle to the SLM.

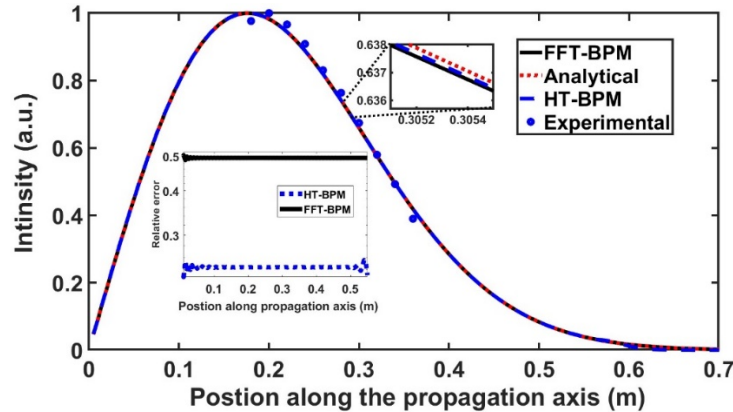


Fig. 9. The axial intensity of the Bessel beam along the propagation axis, the comparison between FFT-BPM and HT-BPM, analytical, and measured experimental results using the setup in Fig. 8, due to the space between the SLM, beam splitter, and beam profiler the measurements started at 0.2 m.

4. Advantages and disadvantages of FFT-BPM and HT-BPM

Here the advantages and drawbacks of FFT-BPM and HT-BPM are discussed.

4.1. FFT-BPM

About advantages, the FFT-BPM has low complexity due to its banded-matrix approximation. It is also efficient in terms of implementation because the fast Fourier transform is widely used and optimized for parallel computers. In the FFT-BPM, there are also no limitations for the system symmetry. In addition, the FFT-BPM can handle a large number of sampling points, allowing for high-resolution simulations [54]. This makes it a powerful tool for studying complex optical systems and analyzing the effects of various parameters on wave propagation. About disadvantages, the FFT-BPM may not be suitable for certain applications that require the use of other discrete transforms, such as the discrete cosine transform, or discrete sine transform. From a numerical point of view, the FFT-BPM is particularly well-suited for systems with a radix 2 power of sampling points [54] (ex. 2^{10} , 2^{11} , ... etc.).

4.2. HT-BPM

About advantages, the HT-BPM is more flexible than the FFT-BPM as it allows for the use of different discrete transforms, such as the discrete cosine transform or discrete sine transform, to locate patterns. This flexibility can be advantageous for certain applications that require specific types of discrete transformations. The execution time is shorter than the FFT-BPM and there is no need for a radix 2 power of sampling points. About disadvantages, it is used only for symmetric

systems due to the limitations of the Hankel transform from 0 to ∞ [33]. In nonsymmetric beam systems, the radial Fourier transform beam propagation method may prove to be the optimal choice. The inherent limitation of the Hankel transform is its reliance on radial and azimuthal symmetry. In the future, we aim to address this limitation by incorporating different models such as the discrete fractional Hankel transform [55–57]. This approach appears promising and could pave the way for further advancements in this field.

5. Persistent need to use BPM in Bessel beam modeling

5.1. Different input beam profiles to generate Bessel beam

The analytical study for most Bessel beam propagations with different light source beam shapes is not available, in such cases a numerical model is highly indigent. For more illustration, Fig. 10 shows the axial intensity profile of the Bessel beam with different input beam profiles: Gaussian and super-Gaussian (flat-top) which have already been discussed by authors [58,59]. The shaping of the input light beam could take other shapes such as Lorentzian and super-Lorentzian. Figure 10 shows a comparison between different input beam profiles: Gaussian, super-Gaussian, Lorentzian, and super-Lorentzian. It can be concluded that by changing the input beam profile, the axial intensity will not remain the same for all cases as in Gaussian and Lorentzian beams, however, it could be a similar profile such as in super-Gaussian and super-Lorentzian cases. Furthermore, in the Bessel beam case, the beam is well collimated so that its angular extent is limited to a narrow region of space around the beam axis, this means that the plane wave components in the spatial spectrum have very small values of the transverse wavenumbers. It is said that K_r is much smaller than K_z , hence high frequencies in the propagated field are negligible.

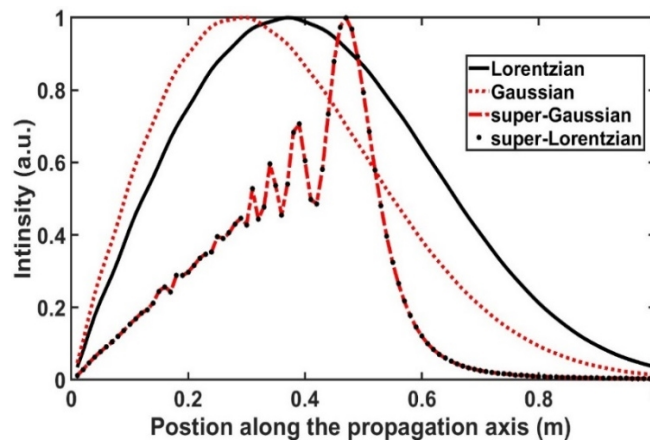


Fig. 10. Axial intensity of the Bessel beam along the propagation axis at different input field profiles: Gaussian, flat-top (super-Gaussian), Lorentzian, and super-Lorentzian.

Moreover, the applications of Bessel beam propagation are extensive and diverse in spanning fields such as optics, acoustics, and electromagnetic waves. The unique properties of Bessel beams, including their non-diffracting and self-healing nature, make them highly desirable for various applications. These applications include optical communications, laser micromachining, optical trapping, propagation through turbulent atmospheres, and medical imaging.

The use of the Hankel transform alongside BPM results in more accurate outcomes for modeling Bessel beams compared to FFT-BPM. The Hankel transform maintains the cylindrical symmetry of Bessel beams, enabling a more precise depiction of their intensity profiles, especially crucial in applications that require precise axial intensity with various shaping structures. Frequently,

to shape axial intensity, the standard equation is altered by integrating the phase of the ring structure. Under these conditions, the Hankel transform is more precise than the Fast Fourier transform in predicting the axial intensity of Bessel beams. Additionally, in applications involving femtosecond Bessel beam drilling, where complex structures like air-to-glass or air-to-silicon transitions are present, a phase correction factor different from unity ($Q(r) \neq 1$) is used. Future research will focus on applications such as optical needles and axial intensity shaping, where HT-BPM is anticipated to be highly accurate and particularly well-suited.

6. Conclusions

In this study, the HT-BPM has been introduced to simulate the propagation of Bessel beams. The HT-BPM exhibits a tenfold increase in speed compared to the FFT-BPM. While the FFT-BPM achieves an accuracy of 89.9% in determining the Bessel beam spot radius relative to the analytical value, HT-BPM achieves 99% accuracy. Comparisons of axial intensity between HT-BPM and FFT-BPM for both analytical and experimental values were conducted across various propagation distances including meters, centimeters, and micrometers. The results indicate that HT-BPM provides a more accurate prediction of the Bessel beam's axial intensity with a smaller relative error compared to FFT-BPM for analytical and experimental data. Additionally, HT-BPM has been applied to model different input beam shaping, demonstrating that changes in the input beam profile affect axial intensity. Future work will expand this study to include Bessel beams in inhomogeneous media and with varying polarizations of Bessel beams. In conclusion, HT-BPM stands out as a faster and more accurate method for simulating Bessel beams' propagation characteristics as compared to FFT-BPM.

Funding. This work was financially supported by the National Science and Technology Council (NSTC) in Taiwan under number (112-2811-E-006-047).

Acknowledgements. The authors extend their gratitude to Professor L. R. Gamma from the Electronics and Communications Department, Faculty of Engineering, Benha University, for his insightful suggestions and enlightening discussions. Additionally, they express their appreciation to Prof. Miroslav Kolesik for the valuable information provided in his course OPTI-547 on the beam propagation method, at the College of Optical Sciences, University of Arizona.

Disclosures. The authors declare that there are no conflicts of interest related to this article.

Author Contributions: A.S.A. Elsharkawi: writing original draft, conceptualization, formal analysis; I. C. Tsai and X. T. Lin: building the optical system integrated with SLM for experiments; C.Y. Chang and Y.L. Lo: conceptualization, formal analysis, investigation, review, and editing.

Data availability. All data generated or analyzed during this study are included in this manuscript.

References

1. J. Durnin, "Exact solutions for nondiffracting beams. I. The scalar theory," *J. Opt. Soc. Am. A* **4**(4), 651–654 (1987).
2. S. Zhao, W. Zhang, L. Wang, *et al.*, "Propagation and self-healing properties of Bessel-Gaussian beam carrying orbital angular momentum in an underwater environment," *Sci. Rep.* **9**(1), 2025 (2019).
3. C. T. Sosa-Sánchez, S. A. Juárez-Reyes, C. Rickenstorff-Parrao, *et al.*, "Superposition of Bessel beams: geometrical wavefronts, light rays, caustic, intensity patterns and experimental generation," *J. Opt.* **20**(8), 85608 (2018).
4. S. N. Khonina, N. L. Kazanskiy, S. V. Karpeev, *et al.*, "Bessel Beam: Significance and Applications—A Progressive Review," *Micromachines* **11**(11), 997 (2020).
5. Y. Matsuoka, Y. Kizuka, and T. Inoue, "The characteristics of laser micro drilling using a Bessel beam," *Appl. Phys. A* **84**(4), 423–430 (2006).
6. P. Muys and E. Vandamme, "Direct generation of bessel beams," *Appl. Opt.* **41**(30), 6375 (2002).
7. J. Durnin, J. J. Miceli, and J. H. Eberly, "Diffraction-free beams," *Phys. Rev. Lett.* **58**(15), 1499–1501 (1987).
8. M. Baliyan and N. K. Nishchal, "Generating scalar and vector modes of Bessel beams utilizing holographic axicon phase with spatial light modulator," *J. Opt.* **25**(9), 95702 (2023).
9. F. Gori, G. Guattari, and C. Padovani, "Bessel-Gauss beams," *Opt. Commun.* **64**(6), 491–495 (1987).
10. M. Dallaire, N. McCarthy, and M. Piché, "Spatiotemporal bessel beams: theory and experiments," *Opt. Express* **17**(20), 18148–18164 (2009).
11. Z. Zhai, Z. Cheng, Q. Lv, *et al.*, "Tunable Axicons Generated by Spatial Light Modulator with High-Level Phase Computer-Generated Holograms," *Appl. Sci.* **10**(15), 5127 (2020).
12. J. A. Davis, J. Guertin, and D. M. Cottrell, "Diffraction-free beams generated with programmable spatial light modulators," *Appl. Opt.* **32**(31), 6368–6370 (1993).

13. M. Aakhte, E. A. Akhlaghi, and H. A. J. Müller, “SSPIM: A beam shaping toolbox for structured selective plane illumination microscopy,” *Sci. Rep.* **8**(1), 1–12 (2018).
14. P. Li, Y. Zhang, S. Liu, *et al.*, “Generation and self-healing of vector Bessel-Gauss beams with variant state of polarizations upon propagation,” *Opt. Express* **25**(5), 5821–5831 (2017).
15. N. A. Ferlic, M. van Iersel, D. A. Paulson, *et al.*, “Propagation of Laguerre-Gaussian and Im-Bessel beams through atmospheric turbulence: A computational study,” in *Laser Communication and Propagation through the Atmosphere and Oceans IX*, J. A. Anguita, J. P. Bos, and D. T. Wayne, eds. (SPIE, 2020), **11506**, p. 115060H.
16. J. He, W.-S. Dan, J.-H. Chen, *et al.*, “Propagation characteristics of a ring Airyprime vortex beam and an Airyprime vortex beam array in atmospheric turbulence,” *Results Phys.* **62**, 107827 (2024).
17. W. Cheng, J. W. Haus, and Q. Zhan, “Propagation of vector vortex beams through a turbulent atmosphere,” *Opt. Express* **17**(20), 17829–17836 (2009).
18. G. M. Balasubramaniam, R. Kumar, and S. Arnon, “Vortex Beams and Deep Learning for Optical Wireless Communication Through Turbulent and Diffuse Media,” *J. Lightwave Technol.* **42**(10), 3631–3641 (2024).
19. P. Birch, I. Ituen, R. Young, *et al.*, “Long-distance Bessel beam propagation through Kolmogorov turbulence,” *J. Opt. Soc. Am. A* **32**(11), 2066–2073 (2015).
20. A. Shaaban, M. F. O. Hameed, L. R. Gomaa, *et al.*, “Accurate calculation of Goos-Hänchen shift at critical angle for complex laser beam profiles using beam propagation method,” *Optik* **157**, 1106–1114 (2018).
21. L. R. Gomaa, A. Shaaban, M. F. O. Hameed, *et al.*, “Competitiveness of the BPM in studying the optical beams at critical incidence on dielectric interfaces,” *Opt. Quantum Electron.* **49**(2), 51 (2017).
22. A. Shaaban, Y.-C. Du, and L. R. Gomaa, “Effects of smoothing functions on the transformation of TM to TE propagation problems in the framework of FFT-BPM: A comparative study,” *Opt. Commun.* **478**, 126374 (2021).
23. G. Lifante, *Integrated Photonics* (2004), 90.
24. S. Jiménez-Gambín, N. Jiménez, J. M. Benlloch, *et al.*, “Generating Bessel beams with broad depth-of-field by using phase-only acoustic holograms,” *Sci. Rep.* **9**(1), 1–13 (2019).
25. M. Scalora and M. E. Crenshaw, “A beam propagation method that handles reflections,” *Opt. Commun.* **108**(4-6), 191–196 (1994).
26. M. D. Feit, J. A. Fleck, and A. Steiger, “Solution of the Schrödinger equation by a spectral method,” *J. Comput. Phys.* **47**(3), 412–433 (1982).
27. M. Shalaby, “Transformation of the three-dimensional beam propagation method to two dimensions for cylindrically symmetric structures based on the Hankel transform,” *Pure Appl. Opt.* **5**(6), 997–1004 (1996).
28. L. Novotny and B. Hecht, *Principles of Nano-Optics* (Cambridge university press, 2012).
29. A. Fathallah and M. Shalaby, “Generalized Bessel beams in modified axially symmetric graded index structures,” *Appl. Opt.* **50**(19), 3128–3134 (2011).
30. F. Courvoisier, P.-A. Lacourt, M. Jacquot, *et al.*, “Surface nanoprocessing with nondiffracting femtosecond Bessel beams,” *Opt. Lett.* **34**(20), 3163–3165 (2009).
31. S. N. Khonina, N. L. Kazanskiy, P. A. Khorin, *et al.*, “Modern Types of Axicons: New Functions and Applications,” *Sensors* **21**(19), 6690 (2021).
32. Z. Jaroszewicz, A. Burvall, and A. T. Friberg, “Axicon - the Most Important Optical Element,” *Opt. Photonics News* **16**(4), 34 (2005).
33. H. F. Johnson, “An improved method for computing a discrete Hankel transform,” *Comput. Phys. Commun.* **43**(2), 181–202 (1987).
34. N. Baddour and U. Chouinard, “Matlab Code for the Discrete Hankel Transform,” *J. Open Res. Softw.* **5**(1), 4 (2017).
35. I. Golub and T. Mirtchev, “Absorption-free beam generated by a phase-engineered optical element,” *Opt. Lett.* **34**(10), 1528–1530 (2009).
36. R. Stoian and J. Bonse, *Ultrafast Laser Nanostructuring: The Pursuit of Extreme Scales* (Springer Nature, 2023), **239**.
37. J. Durnin, J. J. Miceli, and J. H. Eberly, “Comparison of Bessel and Gaussian beams,” *Opt. Lett.* **13**(2), 79–80 (1988).
38. A. S. Rao and G. K. Samanta, “On-axis intensity modulation-free, segmented, zero-order Bessel beams with tunable ranges,” *Opt. Lett.* **43**(13), 3029–3032 (2018).
39. Y. Yang, “High throughput direct writing of a mesoscale binary optical element by femtosecond long focal depth beams,” *Light Adv. Manuf.* **4**(4), 466 (2023).
40. Y. Fan, B. Cluzel, M. Petit, *et al.*, “2D Waveguided Bessel Beam Generated Using Integrated Metasurface-Based Plasmonic Axicon,” *ACS Appl. Mater. Interfaces* **12**(18), 21114–21119 (2020).
41. N. Chattrapiban, E. A. Rogers, D. Cofield, *et al.*, “Generation of nondiffracting Bessel beams by use of a spatial light modulator,” *Opt. Lett.* **28**(22), 2183–2185 (2003).
42. J. A. Davis, E. Carcole, and D. M. Cottrell, “Range-finding by triangulation with nondiffracting beams,” *Appl. Opt.* **35**(13), 2159–2161 (1996).
43. K. Dholakia, M. MacDonald, and G. Spalding, “Optical tweezers: the next generation,” *Phys. World* **15**(10), 31–35 (2002).
44. U. M. S. Andrade, A. M. Garcia, and M. S. Rocha, “Bessel beam optical tweezers for manipulating superparamagnetic beads,” *Appl. Opt.* **60**(12), 3422–3429 (2021).
45. V. V. Kotlyar, A. A. Kovalev, and A. P. Porfirev, “An optical tweezer in asymmetrical vortex Bessel-Gaussian beams,” *J. Appl. Phys.* **120**(2), 23101 (2016).

46. V. Grillo, J. Harris, G. C. Gazzadi, *et al.*, "Generation and application of Bessel beams in electron microscopy," *Ultramicroscopy* **166**, 48–60 (2016).
47. W. Yu, Z. Ji, D. Dong, *et al.*, "Super-resolution deep imaging with hollow Bessel beam STED microscopy," *Laser Photonics Rev.* **10**(1), 147–152 (2016).
48. H. Wang, F. Zhang, and K. Ding, and others, "Non-diffraction-length Bessel-beam femtosecond laser drilling of high-aspect-ratio microholes in PMMA," *Optik* **229**, 166295 (2021).
49. I. Alexeev, K.-H. Leitz, A. Otto, *et al.*, "Application of Bessel beams for ultrafast laser volume structuring of non transparent media," *Phys. Procedia* **5**, 533–540 (2010).
50. F. Courvoisier, "Nonstandard Light for Ultrafast Laser Microstructuring and Nanostructuring," in *Ultrafast Laser Nanostructuring: The Pursuit of Extreme Scales*, R. Stoian and J. Bonse, eds. (Springer International Publishing, 2023), pp. 581–621.
51. F. Courvoisier, J. Zhang, M. K. Bhuyan, *et al.*, "Applications of femtosecond Bessel beams to laser ablation," *Appl. Phys. A* **112**(1), 29–34 (2013).
52. R. Stoian, M. K. Bhuyan, G. Zhang, *et al.*, "Ultrafast Bessel beams: advanced tools for laser materials processing," *Adv. Opt. Technol.* **8**(6), 535 (2018).
53. X. Liu, R. Clady, D. Grojo, *et al.*, "Engraving Depth-Controlled Nanohole Arrays on Fused Silica by Direct Short-Pulse Laser Ablation," *Adv. Mater. Interfaces* **10**(7), 2202189 (2023).
54. A. Shaaban, M. Sayed, M. F. O. Hameed, *et al.*, "Fast parallel beam propagation method based on multi-core and many-core architectures," *Optik* **180**, 484 (2019).
55. M. T. Hanna, "A discrete fractional Hankel transform based on the eigen decomposition of a symmetric kernel matrix of the discrete Hankel transform," in *2017 IEEE 60th International Midwest Symposium on Circuits and Systems (MWSCAS)* (2017), pp. 479–482.
56. M. T. Hanna, "Discrete fractional Hankel transform based on a nonsymmetric kernel matrix," *Digit. Signal Process.* **126**, 103431 (2022).
57. V. Namias, "Fractionalization of Hankel Transforms," *IMA J. Appl. Math.* **26**(2), 187–197 (1980).
58. J. Turunen, A. Vasara, and A. T. Friberg, "Holographic generation of diffraction-free beams," *Appl. Opt.* **27**(19), 3959–3962 (1988).
59. R. Dharmavarapu, S. Bhattacharya, and S. Juodkazis, "Diffractive optics for axial intensity shaping of Bessel beams," *J. Opt.* **20**(8), 85606 (2018).